Waves and transport in the pure electron plasma

J. S. deGrassie[a] and J. H. Malmberg

Department of Physics, University of California, San Diego, La Jolla, California 92093
(Received 21 September 1978; accepted 3 October 1979)

Investigations of low frequency waves and transport in a plasma consisting almost purely of electrons are presented here. This plasma is trapped in a cylindrical system with radial confinement supplied by a strong axial magnetic field and axial confinement supplied by electrostatic fields. Very long containment times are possible. Classical transport due to electron-neutral collisions has been investigated and good agreement with the theory of Douglas and O'Neil is obtained. Externally launched diocotron waves are investigated. The modal frequencies agree well with linear theory, but the damping is governed by nonlinear effects. Experimental scaling laws for the damping rates are given. Measurements of spatial transport due to these modes are also presented. A signature of this process is that the transport is strongly localized spatially.

I. INTRODUCTION

Plasmas consisting of a single charge species are the subject of current research[1,2] both for their intrinsic interest and for the investigation of basic phenomena common to all plasmas. Here, we report experimental investigations of a newly realized plasma equilibrium, the so-called pure electron plasma.[3] Our experimental geometry is cylindrical. The plasma, consisting almost entirely of electrons, is radially confined by a strong uniform axial magnetic field and captured axially by electrostatic fields. This plasma is easy to make, it can be confined by fields of relatively simple geometry, and it is found to have excellent reproducibility properties.

We have previously described[4] the plasma source and the principle behind its design. The source is merely a spiral of thoriated tungsten wire which is heated by passing a direct current through it, and which thermionically emits electrons. This spiral cathode is immersed in the magnetic field and produces a column of electron plasma. The spiral geometry plus the voltage drop due to the heater current provide a first approximation to a match between the cathode electrostatic potential and the potential arising from the space charge electric field of a uniform density electron column.

In a prior experiment[4] we have verified the theoretically predicted[5] dispersive properties of the azimuthally symmetric plasma waves in this plasma. There, we proved that the level of ion contamination is indeed small, that is, the plasma is almost purely electrons. In that experiment the system was operated steady state. For the experiments reported here we have modified the system to capture the plasma axially by closing the ends with electric fields. In a cycle, which is continuously repeated, the machine is filled with electron plasma which is then captured and later dumped. The dumped plasma is collected. One of our primary measurements is of the radial density profile of these dumped electrons.

The experiments described here deal with two basic subjects: waves and transport. For wave investigations, wall probes are used for reception and transmission of waves in the captured pure electron plasma. Here, our work focuses on the low frequency ($\omega \lesssim \omega_p \ll \omega_c$) drift-type modes of this plasma which are known as the diocotron modes.[6-13] To our knowledge, this is the first reported experimental investigation of externally launched diocotron modes. Our results show that linear theory essentially correctly gives the real part of the modal frequency. However, in this experiment the wave damping is governed by nonlinear effects; the amplitude of the wave is large in the sense that resonant electrons execute nonlinear "bounce" orbits which are spatially localized.[13] Clear experimental scaling laws are found for the damping, but a detailed theory is not yet available.

This plasma is ideal for many transport investigations because the basic containment is assured and transport causing effects can be externally induced and controlled. The assurance of the containment stems from the constraint imposed by conservation of canonical angular momentum in a strongly magnetized singly charged plasma. For gross plasma transport, an external torque must be applied. Of course, this torque can be applied by electron collisions with background neutrals or through imperfections in the confining fields. Yet these effects can be rendered ineffectual for time scales appropriate for other induced transport investigations. Indeed, decay times the order of minutes have been obtained with an ultrahigh vacuum version of the system described in this manuscript.

For the induced transport experiments described here, torque has been applied to the plasma in two different ways. First, we investigate "classical" transport due to electron collisions with neutral gas particles. To isolate this process, a gas is bled into the vacuum chamber to raise the neutral density far above the base level. We find that the resulting spatial plasma transport across the magnetic field exhibits the "classical" scaling of decay time, $\tau \propto B_0^2/\nu_{e0}$ where B_0 is the magnetic field strength and ν_{e0} is the electron-neutral collision rate. Transport in this plasma is strongly affected by the space charge electric field.

[a] Present address: General Atomic Company, San Diego, Calif. 92138.

 0031-9171/80/010063-19$00.90

Comparison of radial density profiles with profiles computed from the recent kinetic theoretical treatment of Douglas and O'Neil[14] gives good agreement. Second, torque has been applied by externally launching diocotron modes. These experiments are performed at base pressure to minimize the effect of electron-neutral collisions. A marked signature of this wave induced transport is its spatial localization near the radius at which the wave electric field is in resonance with the zero-order particle drift motion.

We also find regimes in the operating parameters in which strong diocotron modes are naturally excited and cause relatively violent spatial transport. Since this process is internal to the plasma, one expects the resulting transport only to rearrange the distribution function subject to the canonical angular momentum constraint. This is clearly demonstrated for the diocotron wave of lowest azimuthal mode number.

The organization of this manuscript is the following: Section II describes the experimental apparatus and techniques. In Sec. III we describe classical transport due to electron-neutral collisions. The properties of launched waves are described in Sec. IV. Here, the emphasis is on the two diocotron waves of lowest azimuthal mode number ($l=1, l=2$). The measured properties of these two modes differ significantly because in one case ($l=1$) there are no exactly resonant particles. Section V describes the spatial transport induced by the launched diocotron waves and Sec. VI describes transport due to naturally occurring diocotron waves. Section VII summarizes the results.

II. APPARATUS AND TECHNIQUES

First, we briefly review the physics behind the design of the spiral cathode[4] source which determines the properties of the initially captured pure electron plasma. The basic experimental apparatus is depicted schematically in Fig. 1. The geometry is cylindrical and the system is evacuated to a base pressure of approximately 10^{-7} Torr. The spiral cathode is indicated.

Debye shielding in the non-neutral plasma has been treated by Davidson.[15] To be considered a plasma, a collection of electrons must have a Debye length λ_D much smaller than the radius of the electron column. Here, $\lambda_D^2 \equiv \epsilon_0 k_B T/ne^2$, where n is the electron number density, $-e$ is the electron charge, T is the plasma temperature, and k_B and ϵ_0 are Boltzmann's constant and the permittivity of free space, respectively. For the single charge species plasma this means that the plasma potential energy, due to space charge, must be large compared with the thermal energy. A means of producing such a plasma is to tailor the cathode electrostatic potential. The space charge potential ϕ_s, inside a uniform density electron column, varies as $\phi_s \sim r^2$, where r is the radial distance. By using a cathode with potential ϕ_c, varying as $\phi_c \sim r^2$, one might hope to obtain a "match" across the electron column, thus leaving the electrons with a kinetic energy characteristic of the cathode temperature. The spiral cathode approximates this condition. The resistive voltage along the spiral, due to the heater current, produces the potential variation with r.

Experimentally, we find that the potential match is roughly satisfied. For the uniform density electron column one can show that $(\rho/\lambda_D)^2 = 4e\Delta\phi_s/k_B T$ (Ref. 4). Here, ρ is the radius of the column and $\Delta\phi_s$ is the change in space charge potential across the column. The "temperature" will not be a true temperature since the plasma is not initially in thermal equilibrium. The initial kinetic energy is determined primarily by differences between the spiral ϕ_c and the plasma ϕ_s (Ref. 4). Electron-electron collisions can subsequently bring the plasma to thermal equilibrium.[16] Typical initial conditions used in this experiment are $\phi_s(r=0) \sim -20$ V with $\phi_s(0) - \phi_c(0) \sim 1$ V. Also, since the spiral cathode potential is only approximately parabolic and the electron emission is nonuniform due to gaps, the radial profile of the initial plasma is only approximately uniform.

Other elements of the source shown in Fig. 1 are the grid and backplate. The grid is grounded while the cathode is negatively biased and serves to increase the perveance of the source. The backplate is at the potential of the most negative part of the spiral (the center) and thus reflects source electrons.

Now consider the captured plasma. The plasma is shown captured in the region of conducting cylinder B in Fig. 1. Radial confinement is provided by the strong axial magnetic field, B_0, and axial confinement is due

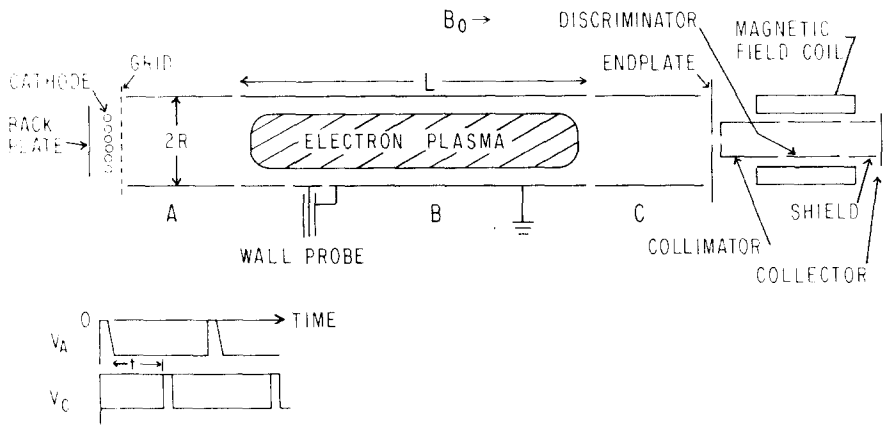

FIG. 1. Schematic diagram of the apparatus. Dimensions are $R = 3.40$ cm, $L = 45.7$ cm, collimator diameter $= 0.30$ cm.

to electrostatic fields between cylinder B and the conducting cylinders A and C. Cylinders A and C are biased sufficiently negative such that it is energetically impossible for the electrons to escape longitudinally, that is, $\phi_A, \phi_C \ll \phi_s$. In order to escape, the captured electrons must cross the magnetic field lines, reach the wall of cylinder B and be absorbed.

The system is continuously cycled by filling B with electron plasma from the source and subsequently dumping it out the other end. More specifically, this sequence is as follows (see insert in Fig. 1 which sketches the applied voltages): (1) Initially, A is grounded and C is biased negatively with respect to the source so that those electrons from the source which reach B are reflected at C. During this phase the plasma occupies cylinders A and B and the plasma density is primarily determined by the source potential and the space charge potential match. (2) Then, the potential of A is gated negative to trap the plasma within B. The trapped electrons wander across the magnetic field lines due to various processes. A variable time (t) later, cylinder C is gated to ground potential, dumping the remaining electrons out that end along the magnetic field lines to be collected. This sequence is repeated continuously with repetition rates ranging from 1 to 100 cycles/sec, depending upon the process under investigation. For clarity, only three cylinders are indicated in Fig. 1, whereas the machine actually contains five.

A radially moveable collector assembly behind a slot in the end plate collimates and collects the dumped electrons at the radial (r) and azimuthal (θ) position of the collimator. The charge collected at each dump produces a voltage across the distributed capacitance (C_d) of the collector element. This voltage is proportional to the electron density n, assuming the density to be longitudinally independent in the captured plasma. The collector is connected to ground through a drain resistor R_d and so the voltage signal subsequently decays with an R_dC_d time constant (typically $R_dC_d \sim 10^{-3}$ sec). The peak voltage is sampled and held for display on an xy recorder.

The radial position of the collector assembly is transduced and applied to the x axis of the recorder, by varying r we obtain $n(r)$ and changing the dump time yields $n(r, t)$. Thus, we measure the time evolution of the plasma density profile as the plasma undergoes transport across the magnetic field. The time t is measured with an interval timer whose digital output is converted to an analog voltage for occasions when t is a desired recorder variable.

With this density measuring technique, irreproducibility from shot-to-shot will produce "noise" in the recorder ordinate. Examples of radial density profiles exhibiting good reproducibility are shown in Fig. 2. Irreproducibility would cause large variations in the density with a fixed collector position. Here, this position is varied slowly (approximately 30 sec for a scan) compared with the repetition rate of 60 sec^{-1}. Note that here the nonuniform initial profiles are due to strong radial transport, as described in Sec. III.

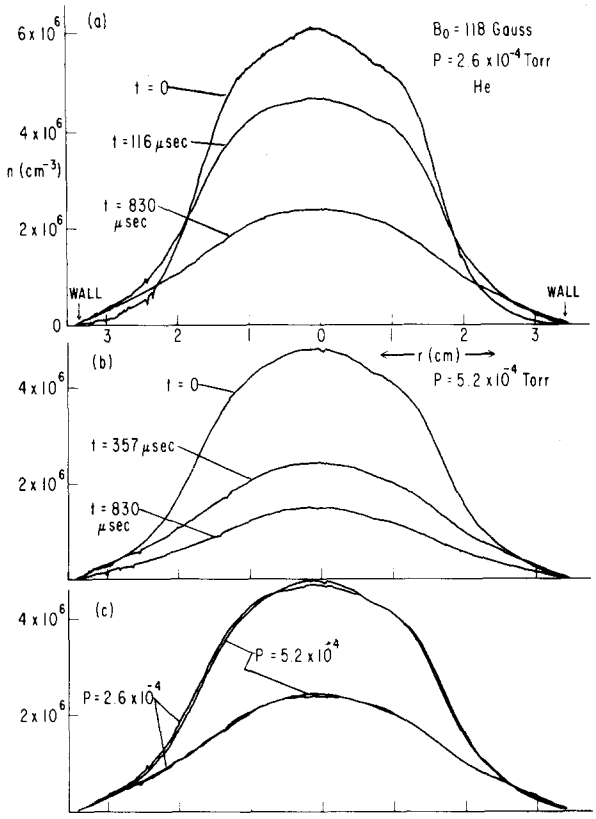

FIG. 2. Transport due to electron-neutral collisions; similarity under a change in neutral gas pressure. (a) Low pressure case; (b) high pressure case; (c) profiles from first two graphs which demonstrate $n(r,t,P,B_0)=n(r,Pt,B_0)$.

The azimuthal asymmetry of the plasma is measureable with a collector at a fixed θ because of the $\mathbf{E}^0 \times \mathbf{B}_0$ rotation, where $\mathbf{E}_0$ is the space charge electric field, $\mathbf{E}^0 = -\nabla\phi_s$. Varying t by a fraction of the rotation period (of order 10^{-6} sec) has the same effect as changing the angular position of the collector. However, the electron plasma rotates at some varying rate during the dump processes and this tends to wash out the azimuthal information measured at the collector. This effect depends upon the dynamics of the dump process, which has not yet been investigated in detail. Nevertheless, angular density perturbations can be measured. We estimate from model calculations that these perturbations are washed out to approximately one-third the initial value for the data presented here (Sec. VI).

Several methods may be used to obtain the absolute magnitude of a radial profile. We can measure the line density, $N(t) = \int_0^R dr\, 2\pi r n(r, t)$, by wall probe techniques[4] or by measuring the total charge coming out at each dump (R = radius of cylinder). We could also calibrate the radial collector measurement itself. However, we have found that the most convenient way is to measure the frequency of resonance transmission of the diocotron wave of lowest azimuthal mode number. Theory predicts[17] this frequency to be proportional to the line density while experimentally we observe this proportionality to within a few percent (Sec. IV).

Waves are launched and received with wall probe

antenna. Located throughout cylinder B are five wall probes like the one shown schematically in Fig. 1. These probes are rectangular sections of the wall which are electrically isolated from cylinder B and mounted flush with its inner surface. Image currents flow to and from the probe in response to the motion of the electrons within cylinder B. This induced current is proportional to the rate of change of the normal electric field at the probe integrated over the surface of the probe.[18] Consider, for example, the wall probe response to a collective electrostatic mode in the plasma given by a potential perturbation of the form $\delta\phi = \psi(r)\exp(il\theta + ikz - i\omega t)$, where z is the axial coordinate. The induced current I is then given by

$$I = -4i\omega\epsilon_0 R \left.\frac{\partial\psi}{\partial r}\right|_R \frac{\sin l\Delta\theta}{l}\frac{\sin k\Delta z}{k} \times \exp(il\theta_0 + ikz_0 - i\omega t),$$

where θ_0 and z_0 are the azimuthal and axial locations of the center of the probe, and $2(\Delta\theta)$ and $2(\Delta z)$ are the arc and axial extent, respectively, of the probe. Thus, measurement of the magnitude of the induced current and knowledge of the shape of the eigenfunction allows determination of the absolute magnitude of $\psi(r)$. For these probes, $\Delta z = 0.96$ cm, $\Delta\theta = 0.38$ rad and the (z_0, θ_0) locations are $(5.08, 0)$, $(5.08, \pi/2)$, $(5.08, \pi)$, $(13.34, \pi/4)$, and $(40.64, 0)$, where $z_0 = 0$ marks the end of cylinder B nearest the source.

Experimentally, modal frequencies can be recognized by clear resonances in the received power as the frequency of a transmitter is varied. Wall probes are used for such transmission and reception. Measurement of the phase difference between the fixed wall probes restricts the allowable k and l values. These same techniques are applied to naturally occurring modes (not launched) using a narrow band receiver for frequency measurement. Many of these modes have been identified by comparing the measured properties with computations of the dispersion relation by the method described in Sec. IV B.

In this electron plasma, measurements of the velocity distribution are complicated by space charge effects. Although one can certainly measure the velocity distribution of the electrons exiting the confinement region with each dump pulse, it is not, in general, straightforward to then deduce the distribution function of the plasma prior to the dump pulse, when the plasma was axially confined. The electrons leave cylinder B with a parallel kinetic energy determined primarily by the space charge field they experience upon exit. Those escaping first have a kinetic energy comparable to the trapped space charge potential energy while those escaping last just coast out. The energy spread due to this space charge potential energy of the trapped plasma is large compared with the kinetic energy.

In order to gain a qualitative measure of the plasma kinetic energy before the dump, we use the technique of electrostatic energy analysis in conjunction with a nonuniform magnetic field.[19] This allows a measure of the kinetic energy of the electrons perpendicular to the main magnetic field, B_0. This perpendicular energy is negligibly affected by space charge forces because the gyroperiod is very short compared with time scales over which an exiting electron encounters changing fields. The cylinders and magnetic field coil shown in the collector assembly (Fig. 1) are used for this measurement. The magnetic field coil produces a field which opposes the main field, and thus reduces the magnetic field strength within the discriminator cylinder. The electrons experience this field change adiabatically, retaining a constant magnetic moment while converting some perpendicular energy into parallel energy. A retarding voltage applied to the discriminator acts upon the parallel energy. By measuring the collected charge as a function of the discriminator voltage with and without the magnetic field change, we obtain information on the distribution of perpendicular energies. To avoid a possible error in this technique, the analyzer is constructed so that the retarding potential rises more slowly (spatially) than the change in magnetic field strength. Otherwise, electrons with sufficiently large initial pitch angle will be spuriously reflected.

For small changes in the magnetic field this method can be shown[20] to yield the mean perpendicular energy which, in general, is a function of the parallel energy. We observe the dependence on parallel energy to be mild and so use this measurement as a check on "temperature" values inferred by other means. Note that if the plasma velocity distribution were an isotropic Maxwellian, then this perpendicular energy technique would directly measure the distribution, since in this case the mean perpendicular energy is independent of the parallel energy. The space charge effect disrupts only the parallel component of the velocities and so for a Maxwellian, which is separable in its velocity space components, the perpendicular information will be dumped intact. A nearly Maxwellian distribution would be expected for the case of a strongly magnetized pure electron plasma with a high enough electron-electron collision rate.

For the investigation of classical transport due to collisions with neutrals, we bleed gas into the vacuum system. To make the neutral density uniform throughout the system, the valve opening leading to the vacuum pump is greatly restricted. The neutral pressure is increased to a level sufficiently above the base pressure so that effects from electron collisions with impurities are small on the time scales of interest. The neutral density is measured with a Bayard–Alpert ionization gauge and standard calibration values applied for various gases. For this work the absolute magnitude of the neutral density is not as important as reliability of relative magnitudes. Our interest in this initial experiment is to establish that this classical transport process can dominate the pure electron plasma and not to measure electron-neutral scattering cross sections. Schulz has investigated[21] the characteristics of the Bayard–Alpert gauge for helium over the range of interest in this experiment, finding the response linear to within roughly a factor of two from 10^{-5} to 10^{-2} Torr.

Typical parameters at $t=0$ are plasma frequency $\omega_{p0}=[n(0,0)e^2/m\epsilon_0]^{1/2}$ of order 10^8 rad/sec, cyclotron frequency 10^9–10^{10} rad/sec, axial transit time 10^{-6} sec, λ_D of order 0.3 cm, and the electron-neutral elastic collision time is of order 10^{-3} sec at base pressure. Ionizing collisions during the trapped phase are believed to be very rare since the mean electron kinetic energy is well below ionization thresholds. The ion contamination is at most a few percent as measured by wave[4] and image current techniques and model calculations indicate it is probably very much smaller. In the image current method, the net current to the walls is monitored. This current reflects the mean rate of any secondary electron buildup as the ions escape axially.

III. CLASSICAL TRANSPORT DUE TO ELECTRON NEUTRAL COLLISIONS

The first process that we consider is transport due to electron collisions with background neutral gas particles. As implied by the label "classical transport" the physics can be understood by consideration of single electron orbits subject to collisional encounters. Here, torque is applied to the electron plasma by the neutrals via collisions.

The requirement that an external torque is necessary for bulk transport has become a unifying concept for all of our transport investigations. To make this constraint more quantitative consider the canonical angular momentum of the ith electron, $P_{\theta i}=m(rv_\theta - r^2\omega_c/2)_i$. Here, v_θ is the azimuthal component of the velocity of the electron, comprised of the thermal motion and also the drift motion due to the space charge electric field. The total canonical angular momentum of the electron plasma is $P_\theta=\sum_i P_{\theta i}$. If no external torque is applied, then $P_\theta=$ const. For the strongly magnetized case $r\omega_c \gg |v_\theta|$, $P_{\theta i}\simeq -\frac{1}{2}m\omega_c r_{gi}^2$, where r_g is the radius of the guiding center. With no external torque, $P_\theta=$ const requires $\sum r_{gi}^2\simeq$ const. This says that if some electrons increase their average radial position, others must decrease theirs. Such a rearrangement can cause a loss of only a small fraction of the electrons since the initial plasma radius is considerably smaller than R. An external torque must be applied in order to have gross transport to the boundary. Intraplasma forces, such as electron-electron collisions and collective plasma effects, may rearrange the electron distribution but cannot destroy the basic containment. This conservation law does not constrain gross transport in a charge neutral plasma since the contributions to P_θ from the oppositely charged species can cancel in that case; that is, the electrons and ions can cross the field lines together.

A collision of an electron with a neutral applies a torque when $v_{\theta i}$ is changed by the collision process. This causes transport across the magnetic field through the well-known mechanisms of diffusion and mobility.[22] Mobility occurs because the electron drift velocity due to the space charge electric field biases the average electron step in the outward radial direction. This leads to a radial mobility flux. Diffusion results from collisions acting on the electron gyroorbits due to thermal motion. In the pure electron plasma the radial flux due to mobility, Γ_e, dominates the radial diffusion flux, Γ_d, since the plasma space charge energy is large compared with the thermal energy. Locally, $|\Gamma_e/\Gamma_d| \sim ra/\lambda_D^2$ where a is the scale length of the local density gradient.

Recently, a theoretical description of electron-neutral transport in the pure electron plasma has been given by Douglas and O'Neil.[14] They calculate the evolution of the electron distribution function averaged over gyrophase using an expansion of the Boltzmann equation in inverse powers of the magnetic field strength. Their model assumes that the electrons are elastically scattered off stationary infinite mass scatters and also that the distribution function is azimuthally invariant. Electron-electron collisions are neglected.

This collision model is well realized experimentally when helium is the neutral gas. The collisions are elastic since the electron kinetic energy is below the energy necessary to excite or ionize the helium atom. The inifinte mass approximation is valid since effects due to neutral recoil are small for the time scales of interest in the experiment. Also, the electron-electron collision frequency is orders of magnitude smaller than the electron-neutral collision frequency for the parameters of this experiment.

The Boltzmann equation is required to describe this transport because the distribution function becomes highly non-Maxwellian through the processes of diffusion cooling and Joule heating. Diffusion cooling arises because the fastest electrons diffuse out first while Joule heating is due to the gain in kinetic energy of an electron as it moves radially outward in the presence of the space charge electric field. Electron collisions with infinitely massive neutrals do not make the distribution Maxwellian but can make it isotropic.

The Douglas–O'Neil theory results from an expansion of the Boltzmann equation in two small parameters, ϵ and δ, where $\epsilon \sim r_L/r$, $E^0/(B_0\bar{v})$ and $\delta \sim \nu_{e0}/\omega_c$ with ordering $\delta \lesssim \epsilon \ll 1$. Here, r_L is the Larmor radius, $\bar{v}$ is the mean electron random speed, and ν_{e0} is the electron-neutral collision frequency. Typical experimental values for these ratios are $r_L/R \sim 10^{-2}$, $E^0/B_0\bar{v} < 10^{-1}$, and $\nu_{e0}/\omega_c \sim 10^{-4}$.

The Douglas–O'Neil reduced transport equation for $f(r,v,t)$ is[14]

$$\frac{\partial f}{\partial t}=\frac{n_0}{3\omega_c^2}\left[\frac{v^3}{r}\frac{\partial}{\partial r}r-\frac{e}{m}E^0\left(4v+v^2\frac{\partial}{\partial v}\right)\right]\sigma_m(v)$$

$$\times\left(\frac{\partial}{\partial r}-\frac{e}{m}E\frac{1}{v}\frac{\partial}{\partial v}\right)f, \tag{1}$$

where n_0 is the neutral gas density, σ_m is the momentum transfer scattering cross section, and v is the electron speed. The transport description is thus a solution to an initial value problem given by Eq. (1) coupled with determination of E^0 through Poisson's equation

$$\frac{1}{r}\frac{d}{dr}(rE^0) = -\frac{e}{\epsilon_0}\int_0^\infty 4\pi v^2\, dv\, f(r,v,t)\,. \tag{2}$$

First, consider the basic time scaling evident from (1). Time enters only through the product tn_0/ω_c^2 and so the time evolution scales as B_0^2/n_0. This is expected for this classical transport process; the collisions are binary and both the mobility and diffusion processes scale as B_0^2. Experimentally, we measure the lowest moment of f, that is, the density $n(r,t)$ for which the same time scaling holds.

A convincing way in which to demonstrate scaling experimentally is to use the method of similarity. Scaling with neutral density (pressure) implies $n(r,t,P,B_0) = n(r,Pt,B_0)$ and thus, we expect that a given initial density profile will decay as a universal shape when the time is scaled as Pt (constant B_0 and $P \equiv$ neutral pressure). To use similarity, it is not required that density profiles obtained with different background pressures agree at time zero. They need only agree at some time. That is, if $n(r,P_1t_1,B_0) = n(r,P_2t_2,B_0)$, then similarity requires that $n(r,P_1t_1',B_0) = n(r,P_2t_2',B_0)$ with $P_1(t_1'-t_1) = P_2(t_2'-t_2)$. We use this approach experimentally because density profiles at $t=0$ vary with P (and B_0) due to transport which occurs during the time it takes to "close" cylinder A. The gating pulse which "closes" cylinder A is deliberately slowed (rise time ~100 μsec) to avoid excitation of the $l=1$ diocotron mode. This effect is discussed in Sec. VI.

In Fig. 2 similarity in the decay of $n(r)$ under a change in neutral pressure is shown. The two sets of profiles shown in Figs. 2(a) and 2(b) differ in that they are taken at different neutral gas (helium) densities. The helium pressure for set (b) is twice that of set (a) and as expected, the higher pressure case decays faster. Shown in Fig. 2(c), on the same plot, are the appropriate profiles from Figs. 2(a) and 2(b). The profiles in 2(c) start the same and decay to the same shape on a time scale governed by $P\Delta t = \text{const}$.

The time scaling with B_0 is demonstrated by the same technique and is shown in Fig. 3. Here, the pressure is constant and, for the two sets of profiles in Figs. 3(a) and 3(b), the ratio of the square of the magnetic field strength is two, 3(a) being at the larger B_0. The agreement of the profiles in Fig. 3(c) shows that the profile decay time scale satisfies $\Delta t/B_0^2 = \text{const}$.

Actually, for these similarity results to follow from Eqs. (1) and (2), the distribution, $f(r,v,t)$, for the initially compared cases must be the same. We have not proven this to be the case since we only have an integral measure of the velocity dependence of this distribution. Nevertheless, similarity is seen to hold in these density profiles. This can be understood since mobility is the dominant transport mechanism (depending basically on plasma density) while diffusion alters details of the density profiles

The initial electron density also enters the decay time scale because of the mobility process. The flux due to mobility is proportional to the space charge electric field which in turn is proportional to the electron number density. Thus, larger plasma densities will decay faster. This effect is not as transparent in Eq. (1) as is the neutral density and magnetic field strength scaling. In order to illustrate this mobility process we consider a simple model calculation. This calculation also serves as motivation for the manner in which some data are taken and analyzed.

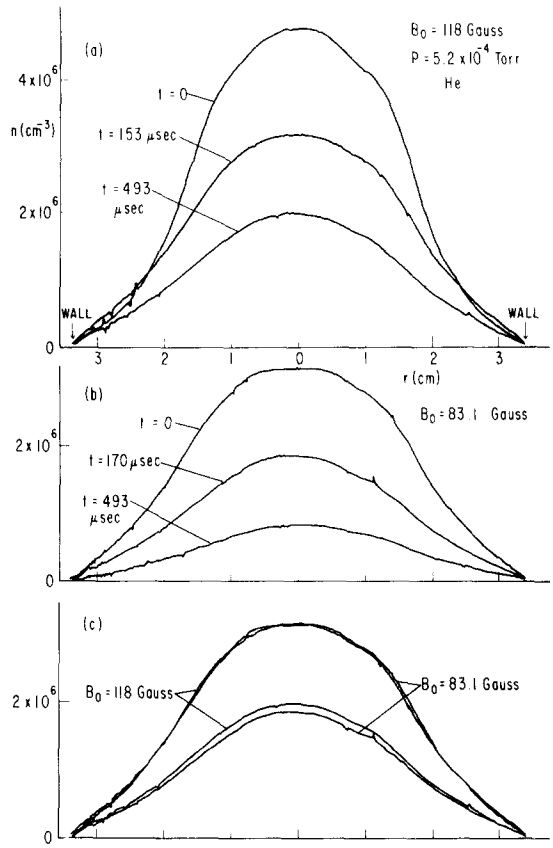

FIG. 3. Transport due to electron-neutral collisions; similarity under a change in B_0. (a) High-field case; (b) low field case; (c) profiles from first two graphs which demonstrate $n(r,t,P,B_0) = n(r,P,t/B_0^2)$.

Consider an initially uniform column of electrons in a strong magnetic field subject to radial transport from mobility alone. We assume that the temperature of the plasma is negligible and introduce a constant electron-neutral collision frequency ν. The radial velocity of the electron fluid is related to the space charge electric field through the usual mobility coefficient (Ref. 22), $\mu = -\nu/B_0\omega_c$, that is, $\mathbf{v} = \mu E^0 = (\nu\omega_p^2/2\omega_c^2)\mathbf{r}$ for a uniform profile. A density profile which satisfies the continuity equation, $\partial n/\partial t + \nabla\cdot(n\mathbf{v}) = 0$, is given by

$$\begin{aligned} &n(r,t) = \bar{n}(t)\{1 - H[r - a(t)]\}\,, \\ &\bar{n}(t)/\bar{n}(0) = (1 + t/\tau_m)^{-1}, \quad a^2(t)\bar{n}(t) = a^2(0)\bar{n}(0)\,, \end{aligned} \tag{3}$$

where $\nu\tau_m = \omega_c^2/\omega_p^2(t=0)$ and H is the Heavyside step function. This solution says that the density profile remains uniform and the outer edge expands. The decay time scale is τ_m, the so-called "mobility time."[14] Note that $1/\bar{n}$ is linearly dependent upon time.

This example is artifical since diffusion is neglected. Even if the plasma were initially cold, Joule heating

due to the electron radial expansion would soon heat the plasma and the resultant diffusion would destroy the sharp edge. However, one might expect that the characteristics of this solution would hold true near the center of the plasma column where the diffusion flux is relatively weak because of the small density gradient. Experimentally, we find that it does. The decay of the central density, $n(0,t)$, has a functional form like that in Eq. (3) on a time scale which is the order of that predicted by the idealized calculation.

The curves shown in Fig. 4 are raw data of $1/n(r=0)$, electronically generated from $n(r=0)$, versus t. The parameter is B_0. The slopes of these lines give a convenient way to parametrize the decay to investigate scaling. We expect

$$1/n(0,t) = [1/n(0,0)](1 + t/\tau_m)$$
$$= 1/n(0,0) + [\nu\omega_p^2(0,0)/n(0,0)\omega_c^2]t .$$

So, we expect $d[1/n(0,t)]/dt \propto \nu/\omega_c^2 \propto n_0/B_0^2$. Thus, we can make use of this simple parametrization technique to investigate scaling over a wide range. Of course, when any parameter is varied over a wide range the plasma temperature and thus collision frequency may change somewhat. The collision rate is determined by the thermal velocity (which is large compared with the drift velocity). Nevertheless, the variation is small enough (less than a factor of 3 in temperature over the full range) so that we observe the basic scaling laws expected.

Scaling with magnetic field strength is shown in Fig. 5 where we plot the initial slope of $1/n(r=0,t)$ versus B_0. The scales are logarithmic and the parameter is background pressure. The straight lines through the data points are drawn by eye and the scaling represented by each line is shown. We see that the basic $1/B_0^2$ scaling well represents the data over a wide range in magnetic field strength and pressure.

Neutral density scaling obtained in the same manner is shown in Fig. 6, the parameter is B_0. The straight lines have a slope of 1, representing linear pressure scaling, and are drawn to allow one to easily see the deviation of the data. The data points give a linear scaling to within a factor of 2 over a variation of two orders of magnitude in background pressure. There is a systematic deviation of the points from the linear law, but this is little more than the order of nonlinearity possible in the pressure measurement.[21] (Two typical error bars for the slope measurements are shown in Fig. 5. We have not used a least-squares fit procedure to obtain the lines in Figs. 5 and 6 since we believe the dominant errors are systematic, not random.)

We now compare a calculation of radial density profiles from the Douglas–O'Neil theory with experiment. This comparison is shown in Fig. 7. The smooth curves are from the numerical solution of the initial value problem of Eqs. (1) and (2). We specify the initial density profile by the $t = 0$ experimental density profile, and an initial "temperature" profile is determined from experiment with the perpendicular energy analyzer technique. We approximate $f(r, v, 0)$ by a local Maxwellian and compute the subsequent density profiles by taking the lowest moment of the numerical solution for $f(r, v, t)$. The boundary condition is $f(R, v, t) = 0$. For the cross section $\sigma(v)$, we use the values cited by Gilardini.[23]

This set of theory profiles is fit to the data by adjusting a single parameter, the magnitude of the initial temperature profile. For this fit $T(r=0, t=0) = 1.0$ eV. The theory is seen to give a good description of the experiment for a time long compared with the electron-neutral collision time, which is the order of 1 μsec.

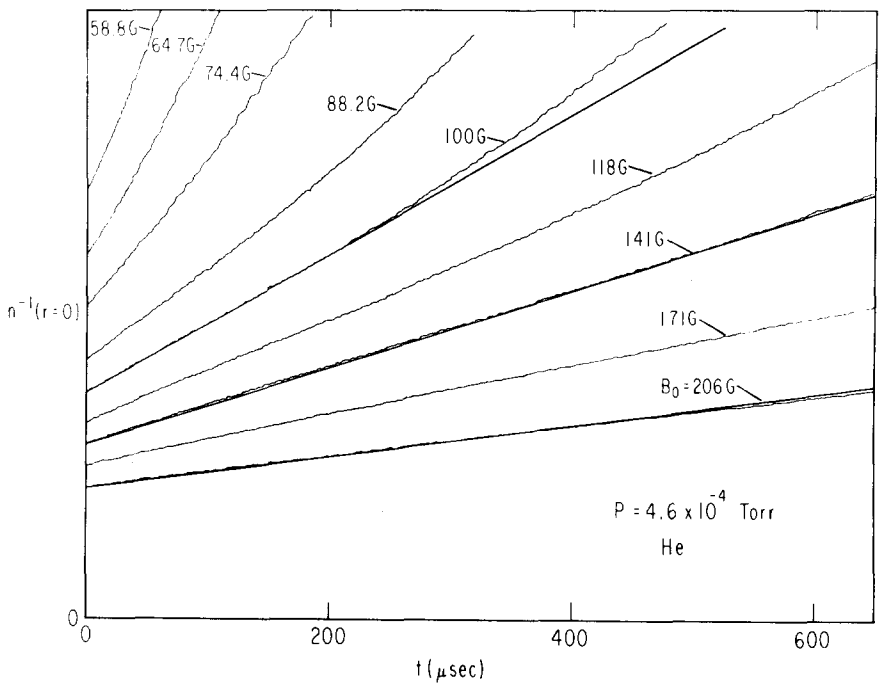

FIG. 4. $n^{-1}(r=0)$ versus time at various B_0 values. Straight lines are drawn by eye through three of the curves to show the linearity.

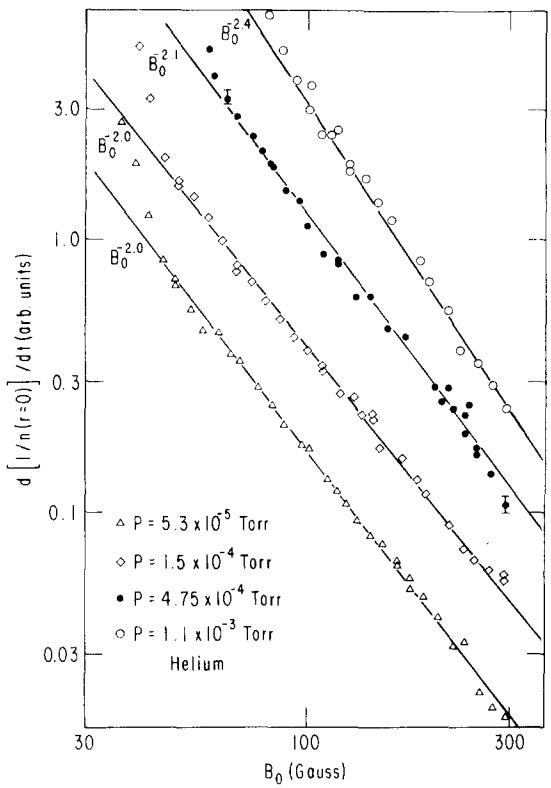

FIG. 5. Transport scaling with magnetic field strength. The ordinate is proportional to the rate of decay of the electron density on axis.

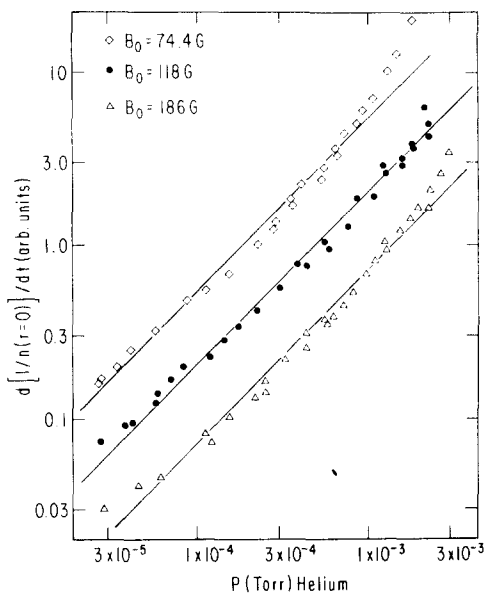

FIG. 6. Transport scaling with background neutral gas density (helium).

The primary dependence of the solution on the temperature parameter is through determination of the time scale for the transport, $\tau \sim 1/\nu_{e0} \sim T^{-1/2}$.

Some of the remaining discrepancy between theory and experiment can be due to the fact that the initial velocity distribution is not a Maxwellian. Because transport occurs during the fill and trapping phases, we expect the distribution at $t=0$ to have the characteristics of a distribution which has undergone Joule heating, as described in Ref. 14. Indeed, the measured initial temperature profile increases with radius. The outer electrons are hotter due to their transport through the larger space charge electric field. The non-Maxwellian nature of the distribution function makes it impossible to assign an absolute "temperature" based upon a measurement of the perpendicular kinetic energy. We use this measurement primarily for corroborative purposes. Nevertheless, comparison of these measurements at various radii probably reflects the correct kinetic energy profile. For the case shown in Fig. 7 this measurement gives the $r=0$, $t=0$ mean perpendicular energy to be 0.6 eV, in reasonable agreement with the value used for the fit.

The results of Douglas and O'Neil show a striking signature in the decay with time of the line density,

$$N(t) = \int_0^R 2\pi r\, dr \int_0^\infty 4\pi v^2\, dv f(r, v, t)\,.$$

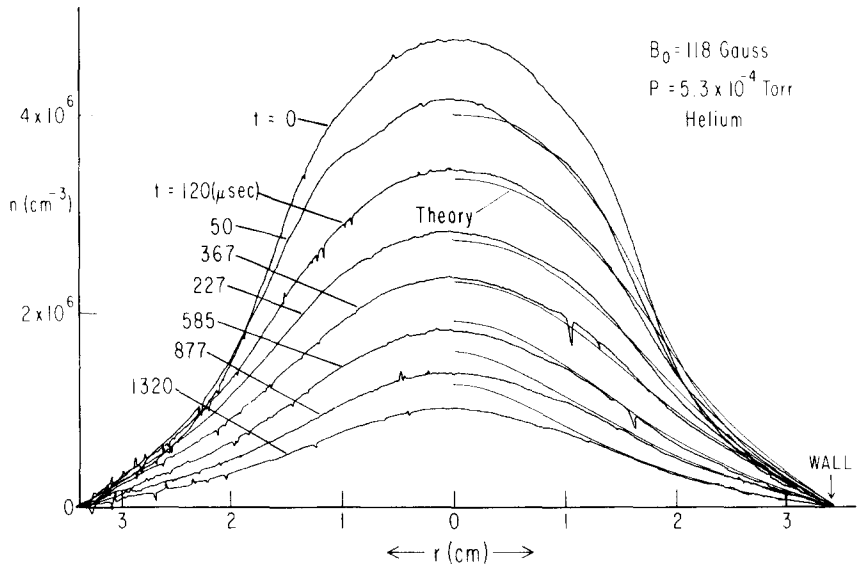

FIG. 7. Comparison of experiment with the theory of Douglas and O'Neil. The smooth curves are from theory. These are from numerical solution of the initial value problem with the $t=0$ experimental profile used as the initial condition.

They find $N(t) \simeq N(0)(1+t/\tau')^{-1}$, a functional form we have encountered in the mobility model calculation. The time scale τ' varies depending upon the ratio $(\lambda_D/a)^2$, where a is the half-width of the initial Gaussian density profile used in their numerical computations. This signature persists over a wide range of values of $(\lambda_D/a)^2$.

Our experimental results also show this signature. Shown in Fig. 8 is the line density N and its reciprocal $1/N$ versus time. The line density is measured by collecting all the charge dumped from the machine and the reciprocal is again taken electronically. The linear portion of the $1/N$ curve demonstrates the theoretical form. Here $(\lambda_D/R)^2 \sim 10^{-2}$, that is, we are in the mobility-dominated regime. Of course, the fact that the decay has this form cannot be purely a mobility effect since there is no mobility flux at the wall where the electron density goes to zero. However, one might expect that the electron temperature at the wall, which determines the diffusion flux there, is governed by the magnitude of the initial space charge electric field. Indeed, we find that the decay rate of the line density depends upon the initial line density: higher densities decay faster.

We note that the time scale for the decay of the line density shown in Fig. 8 is the order of the mobility time one would estimate by assuming a uniform electron density, $\bar{n}$, given by $\pi R^2 \bar{n} = N$. We also find that this time scale shows the expected scaling with B_0 and neutral density, that is, $\tau' \sim B_0^2/P$.

So far, we have been dealing with electron-neutral collisions that are elastic, which is, of course, what is considered by the Douglas–O'Neil theory. Experimentally, we see an interesting contrast when the collisions are inelastic. Here, the electrons lose kinetic energy during collisions, thus removing the energy gained through Joule heating. For an inelastic scatterer we use CO_2. Radial density profiles are shown in Fig. 9. Notice the marked qualitative difference between these profiles and those taken for transport due to elastic collisions in helium (Figs. 2, 3, and 7). Here, the relatively sharp edge of the density profile persists and moves out radially just as in the pure mobility model calculation. The loss of kinetic energy due to the inelastic collisions reduces the diffusion flux relative to the mobility flux so that the edge of the profile is maintained. The kinetic energy measured by the perpendicular energy analyzer for this CO_2 case is small compared with measurements for helim scatterers. For example, at $t = 1554$ μsec and $r = 1.1$ cm this measurement can only put an upper limit on the mean perpendicular energy of 0.2 eV. In contrast, for helium under the same conditions and with the pressure adjusted to give roughly the same decay time this measurement yields an energy of 1.2 eV.

This concludes the discussion of classical transport due to electron collisions with neutrals. We have demonstrated experimentally the expected scaling with neutral density and magnetic field strength and have compared the experimental results to the theory of Douglas and O'Neil, finding good agreement with the theoretical prediction of the evolution of the radial density profiles with time.

IV. LOW FREQUENCY ELECTROSTATIC WAVES

A. Introduction

In this section we describe experimental investigations of low frequency ($\omega \lesssim \omega_p \ll \omega_c$) electrostatic waves in the pure electron plasma. Modes propagating parallel to B_0 are the usual electron plasma waves while those propagating purely in the perpendicular plane are the so-called diocotron waves.[6-13] We shall briefly mention the plasma modes and then focus our attention on the diocotron modes.

Research on the diocotron modes dates back many years to the early stages of the microwave tube industry. The word "diocotron" is often associated with the word "instability." Indeed, all published experimental investigations of these modes deal with waves arising

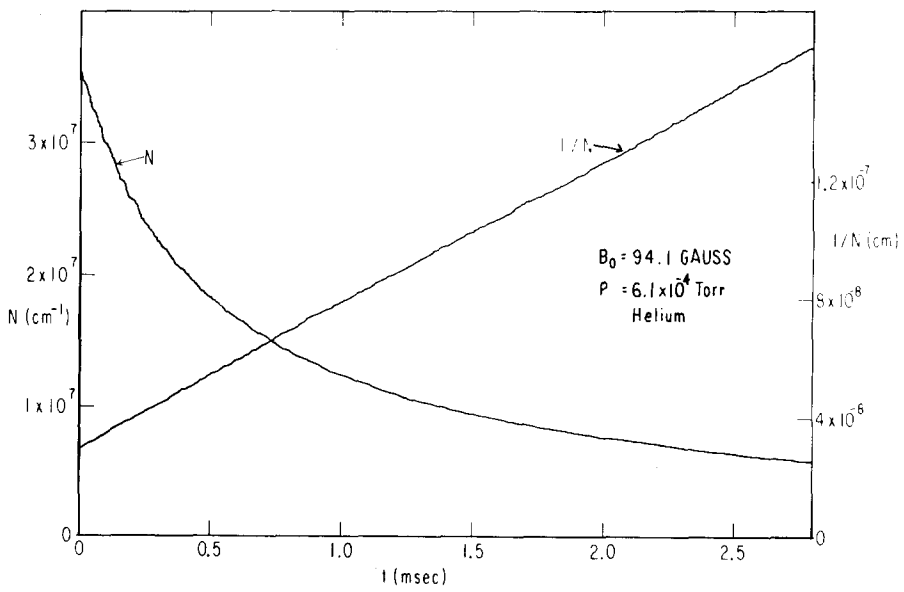

FIG. 8. N and $1/N$ versus t.

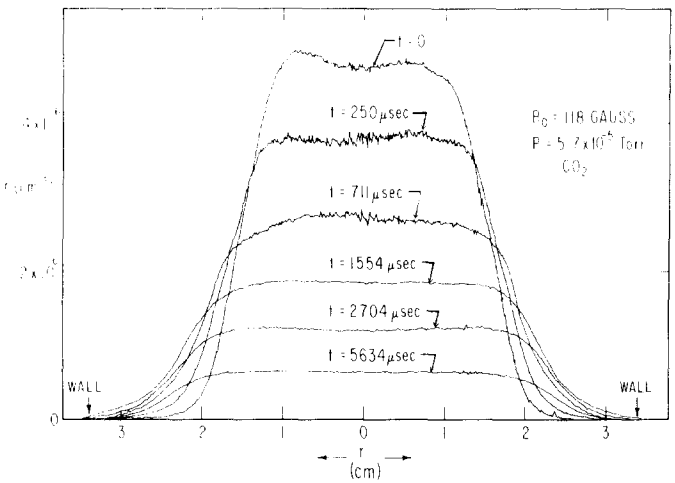

FIG. 9. Radial density profiles for electron-neutral transport with CO_2 as the background scatterer.

due to instabilities. Webster[24] and Cutler[25] observed the breakup of hollow nonrelativistic electron beams due to the diocotron instability and, more recently, Kapentenakos *et al.*[26] described the effect for a hollow relativistic beam. Two experiments on the injection and containment of electrons in toroidal geometry have reported[27,28] diocotron waves arising from injection related instabilities and also an instability triggered by ionization of background gas.

However, as with any collective wave in a plasma, the modal properties can be a separate issue from the plasma properties which may drive the mode unstable. It is of interest to study these diocotron waves in configurations which are stable against their growth. Experimentally, we find that diocotron modes can be excited when a voltage oscillating at the modal frequency is applied to a wall probe. These results are apparently the first reported investigations of externally launched diocotron waves.

B. Theory

The general electrostatic dielectric function for waves in a thermal equilibrium rigid rotor electron plasma has been given by Davidson and Krall.[5] This dispersion relation is derived from the Vlasov description. In our experiment we do not have a thermal equilibrium plasma and must allow for arbitrary density profiles. Linear descriptions of the diocotron modes are usually based upon the fluid approach; that is, using the continuity equation, Poisson's equation, and the drift equation for the electron velocity $v_\perp = (\mathbf{E}\times\mathbf{B}_0)/B_0^2$. Analytic results are generally only available for piecewise uniform density columns.

We find a useful theoretical description in the drift kinetic approach. For low frequencies, the full electron dynamics in the plane perpendicular to $\mathbf{B}_0$ need not be retained. Consider an infinitely long electron plasma column immersed in a strong magnetic field $\mathbf{B}_0 = B_0\hat{z}$. The plasma is specified by the distribution of guiding centers $f(r, v_z, t)$. We assume that all non-wave processes which modify f, such as collisions, are small on the time scale of the wave phenomena of interest. The evolution of f is governed by the drift kinetic and Poisson equations:

$$\frac{\partial f}{\partial t} + \left(\frac{\hat{z}\times\nabla\phi}{B_0}\right)\cdot\nabla f + v_z\frac{\partial f}{\partial z} + \frac{e}{m}\frac{\partial\phi}{\partial z}\frac{\partial f}{\partial v_z} = 0\,,$$
$$\nabla^2\phi = \frac{e}{\epsilon_0}\int dv_z f\,. \tag{4}$$

Assume $f = f^0(r, v_z) + \delta f(r, v_z)\exp(il\theta + ikz - i\omega t)$ and $\phi = \phi^0(r) + \delta\phi = \phi^0(r) + \psi(r)\exp(il\theta + ikz - i\omega t)$. The linearized equation for the eigenvalue ω and eigenfunction ψ is

$$\left(\frac{1}{r}\frac{d}{dr}r\frac{d}{dr} - \frac{l^2}{r^2} - k^2\right)\psi = \frac{e^2}{m\epsilon_0}\left[\int dv_z \frac{k\partial f^0/\partial v_z - (l/r\omega_c)(\partial f^0/\partial r)}{\omega - l\omega_e(r) - kv_z}\right]\psi\,. \tag{5}$$

Here, ω_e is the azimuthal drift frequency, $r\omega_e = (1/B_0)(d\phi^0/dr)$, and $\nabla^2\phi^0 = (e/\epsilon_0)\int dv_z f^0$. Of course, Eq. (5) is valid only for $\gamma \equiv \mathrm{Im}(\omega) > 0$ and weakly damped modes can be recovered by analytic continuation.[13,29] The wave-particle resonance condition is $\omega_r - l\omega_e(r) - kv_z = 0$, where $\omega_r \equiv \mathrm{Re}(\omega)$.

Modes for which $l = 0$ and $k \neq 0$ are the "pure" plasma waves. For these waves the resonance is the usual Landau[29] resonance $\omega_r - kv_z = 0$. As is well known, if the distribution function has a negative (positive) slope at the resonant velocity, the waves damp (grow). This interaction causes velocity space transport which scales as $|\delta\phi|^2$. A description and measurement of such transport is given by Malmberg *et al.*[30] Also, if the wave amplitude is sufficiently large, the resonant electrons are trapped by the wave as described by O'Neil.[31]

Modes for which $l \neq 0$ and $k = 0$ are the "pure" diocotron waves, here, $\delta\mathbf{E} \perp \mathbf{B}_0$. The resonance is spatially localized at the resonant radius r_s, where $\omega_r - l\omega_e(r_s) = 0$. Briggs *et al.*[13] have described the application of the Landau method[29] to this real space resonance. In this case a negative (positive) slope of the density profile at r_s causes the wave to damp (grow). This interaction produces a localized real space transport in second order, an effect not yet discussed theoretically for one-component plasmas. (A related description of such transport in a neutral plasma is given by Stix.[32]) Large amplitude diocotron modes also trap the resonant electrons with the bounce frequency of a deeply trapped electron given by (Ref. 13): $\omega_b^2 = (l^2/r_s B_0)|\psi\, d\omega_e/dr|_{r_s}$.

The $l = 1$ diocotron mode is special in that $r_s = R$, that is, $\omega = \omega_e(R) \propto N/B_0$.[17] No electrons are exactly in resonance with this mode since the density is zero at the wall.

It is useful to reformulate (5) by operating with $\int_0^R r\,dr\,\psi^*(r)$. This gives

$$\int_0^R dr\, r\left[\left|\frac{d\psi}{dr}\right|^2 + \left(\frac{l^2}{r^2} + k^2\right)|\psi|^2\right] + \frac{e^2}{m\epsilon_0} \times \int_0^R dr\, r\left(\int dv_z \frac{k\partial f^0/\partial v_z - (l/r\omega_0)(\partial f^0/\partial r)}{\omega - l\omega_e - kv_z}\right)|\psi|^2 = 0\,. \tag{6}$$

For cases in which $|\gamma/\omega_r| \ll 1$, one can compute γ using the imaginary part of Eq. (6) with $|\psi|^2$ given by the (purely real) eigenfunction resulting from a solution to (5) neglecting resonant particles.

Nothing of the velocity dependence of f^0 need be known in order to numerically solve (5) for the diocotron mode frequencies ($k=0$, $l\neq 0$). However, for the modes with $k\neq 0$ we must specify the velocity dependence of f^0. We assume that f^0 is locally Maxwellian and make use of the plasma dispersion function.[33] By using this Maxwellian approximation to the velocity distribution we can accurately calculate ω_r for the plasma modes while obtaining an approximation for γ.

This calculation assumes a fixed $n^0(r)$ and, thus, is an approximation for cases in which the density profile is perturbed by the wave, as discussed in Sec. V for the $l=2$ diocotron mode. However, this approximation is reasonable in such cases since the real part of ψ is not changed greatly due to a localized change in $n^0(r)$.

C. Experimental

1. Plasma waves

We have previously reported[4] on the dispersion of electron plasma waves ($l=0$, $k\neq 0$) in a steady-state experiment. There, we showed that the dispersion is accurately described by theory and also observed collisionless damping due to the Landau mechanism.

We have also investigated these waves in this captured plasma. Here, the modal frequencies are time dependent since the plasma is decaying in time, continuously changing the dispersion relation. The wave experiments described in this section are performed at base pressure where the time for the central density to decay to one-half its original value is typically 25 msec at $B_0 \sim 180$ G. A mode can be launched by applying a continuous rf voltage to a wall probe at a fixed frequency and observed using another wall probe as a receiver. The received power as a function of time for the lowest axially standing plasma mode, $k=\pi/L$ and $l=0$, is shown in Fig. 10 for four different settings of the transmitter frequency. (The voltage at the transmitter probe was $V_{rms}=0.021$ V.) As the modal frequency sweeps through the transmitter frequency, a resonance in transmission appears. The wave data are taken with the same sample and hold technique as the density data.

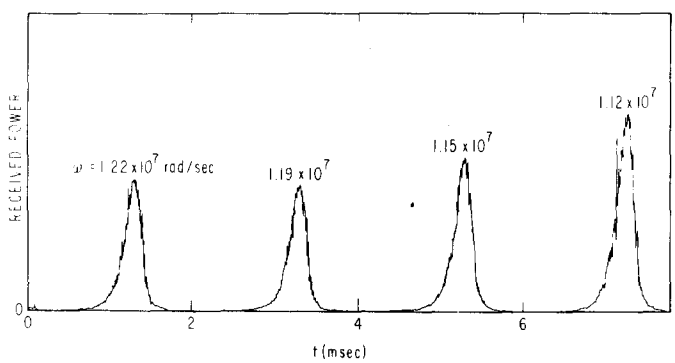

FIG. 10. Received power for an externally launched plasma mode. The transmission for four settings of the transmitter frequency is shown.

We have calculated ω_r from theory using a radial density profile measured at the time of a transmission resonance and obtain a value within 5% of the frequency measured experimentally. With the eigenfunction so determined and the measured absolute magnitude of the received signal, we calculate the wave magnitude within the plasma. For the mode excited at $t=7$ msec, $|\delta n/n|_{r=0}=0.006$.

2. The $l=1$ diocotron mode

Now consider the $l=1$ diocotron mode which is predicted by theory[17] to have the useful property that its frequency ω_r depends only upon the line density N and is independent of the shape of the radial density profile, that is,

$$\omega_r = \frac{-E(R)}{RB_0} = \frac{(e/2\pi\epsilon_0)N}{R^2 B_0} \,. \tag{7}$$

This mode has been observed and used for total charge measurements in two electron injection and containment investigations in toroidal geometry.[27,28] There, the mode was triggered by the injection process itself. We also observe injection related excitation and have found how to avoid this in our system. This will be discussed in Sec. VI.

The received power from an externally launched $l=1$ diocotron mode is shown in Fig. 11. This mode is launched by applying an rf burst, at the modal frequency, to two wall probes. The two received power curves shown in Fig. 11 differ in the length of the applied rf burst. The time t_w is measured from the start of the burst. The plasma responds to the transmitter much like a weakly coupled, lightly damped resonant circuit: the received power rises as t_w^2, the mode can be excited for only a narrow frequency range, Δf, roughly given by $f/\Delta f \sim 40$, and the received amplitude depends linearly upon the rf amplitude applied to the transmitting probes. Notice the persistence of this mode compared with that of the plasma mode shown in Fig. 10.

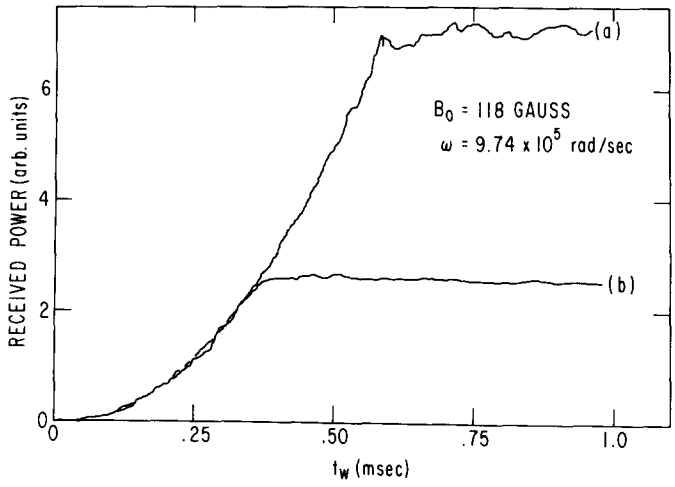

FIG. 11. Received power for a launched $l=1$ diocotron mode. The rf burst length is longer for case (a). The transmitter level is 0.18 V rms and is applied to two wall probes. The maximum received power for (a) corresponds to a peak radial electric field, due to the wave, at the wall probe of 0.76 V/cm.

The relationship between the $l=1$ diocotron mode frequency and the line density is shown in Fig. 12. The decay of the line density with time is shown in Fig. 12(a). Figure 12(b) shows five received power curves superposed on the same graph. Each of these traces is taken in the same manner as those shown in Fig. 11, but the time axis has a much greater span. The modal frequency is measured at a particular time that the transmitter is gated on by measuring the frequency of the transmitter which produces the largest resonance transmission at that time. Then, the curves are taken at these resonant frequencies, which are given in Fig. 12(b). Figure 12(c) shows a plot of the modal frequency (abscissa) versus the line density corresponding to the time at which the received power is maximum. One expects a straight line through the origin as predicted by (7) and we see good agreement in that the points fall within a few percent of the solid line in Fig. 12(c).

The actual measurement shown in Fig. 12(a) is of all the trapped charge Q, since here we measure the total charge dumped from cylinder B (Fig. 1). Now $Q=NeL_t$, where L_t is the length of the trapped plasma. (Actually, L_t is a mild function of radius, but we neglect this here.) To test the predicted dependence of (7), we must know L_t to obtain N. This length depends slightly upon ϕ_s and the potentials applied to cylinders A and C. The solid line drawn in Fig. 12(c) uses a value for L_t (39.4 cm) which is expected[34] for the applied potentials used here and the space charge potential at the time of the $\omega=1.41\times10^6$ rad/sec wave. There is some deviation of the data in Fig. 12(c) from the form predicted by (7). The dotted line shows that the data are better represented by a straight line missing the origin. This effect is not yet understood, but does not seem to be due to the expected variation of L_t with line density.[20]

We use the measured frequency of the $l=1$ diocotron mode to determine the line density through use of Eq. (7). The measured discrepancy shown in Fig. 12(c) is only a few percent for the trapped charge values typically used. Use of the line density measured in this manner to calibrate the radial density profiles allows theoretical calculations of other modal frequencies which agree well with the experimental values. This agreement further strengthens our confidence in this method of determining the plasma line density.

Now consider the imaginary part of the $l=1$ diocotron mode frequency. This mode is predicted by theory to be neutrally stable for a perfectly conducting boundary; but because it is a negative energy mode, a resistive boundary could destabilize it.[13] We calculate this resistive wall effect for our experimental conditions to give a growth time the order of an hour, which is unobservable. Another load upon the wave energy is the power absorbed by the resistively terminated wall probes, but we have not observed growth of this mode for a variety of termination impedances.

A launched $l=1$ diocotron mode damps after the transmitter is gated off, and we have found that a convenient way in which to parameterize the damping data is to plot the log of the received power versus the square of the time after the peak in the received power, t_0. These data are then well fit by a straight line, that is, $|\delta\phi|^2 \sim \exp(-\alpha^2 t_0^2)$. Raw data of such a plot are shown in Fig. 13. The parameter is B_0; the smaller B_0, the faster the decay. The modal frequency differs for each case since $\omega \sim B_0^{-1}$. In these data the receiver gain has been changed to keep the received peak powers the same.

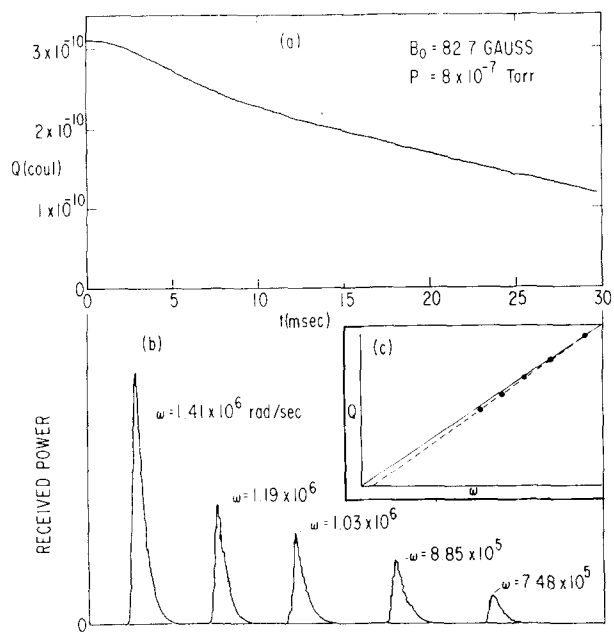

FIG. 12. Dependence of the $l=1$ diocotron mode frequency upon the total trapped charge Q. (a) Q versus t; (b) received power. The rf burst length is 400 μsec. The transmitter frequency giving resonance transmission for each launch time is indicated; (c) plot of Q versus ω. Here, the error bars are smaller than the symbols.

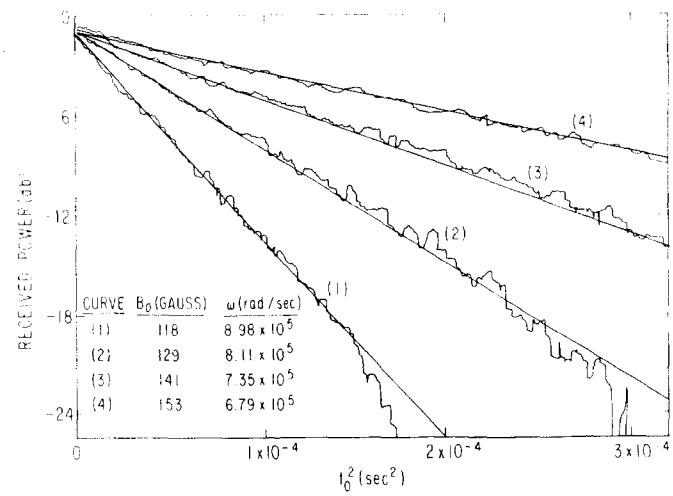

FIG. 13. Received power for launched $l=1$ diocotron mode versus t_0^2 where t_0 = time measured from the peak in received power. Receiver bandwidth = 100 kHz.

(For these data, the damping rate is independent of amplitude.) The lines through the data are drawn by eye and their slopes measure α^2. In Fig. 14 we plot the $1/\alpha^2$ (log scale) so determined versus the log of B_0. The straight line through the data points is determined by a least-squares fit giving the scaling as $(1/\alpha^2) \sim B_0^{5.9}$.

The data shown in Fig. 13 are taken with a relatively broadband receiver. Using a narrow band receiver we find that the frequency of the received wave drops slightly as the wave damps. Typically, this drop is 5% –10%. This is understandable since the plasma line density decays slightly during this time and ω is proportional to N. However, this frequency shift does not appear to be the fundamental cause of the damping since, for certain parameters, there are cases of wave decay with a negligible change in N (< 1%).

Significant changes in the line density at the time the wave is launched do affect the damping. Holding B_0 constant (118 G) and varying N by nearly a factor of 2 we measure the scaling $(1/\alpha^2) \sim N^{-4.9}$. Other factors affecting the damping are the background pressure and L_t. Higher pressures cause the wave to decay faster, with α^2 varying faster than P^2. Increasing L_t (by using a different gating cylinder) increases the damping.

Thus, we find that the real part of the frequency of the $l=1$ diocotron mode can be calculated to good accuracy by the idealized theory assuming an infinitely long electron plasma and keeping only the drift motion perpendicular to B_0. There is a small deviation between theory and experiment of as yet unknown origin. However, to describe the damping of this mode it certainly appears that more of the true electron dynamics must be addressed by theory.

3. Diocotron modes for $l>1$

The properties of diocotron modes of higher l are significantly different from those of the "fundamental"

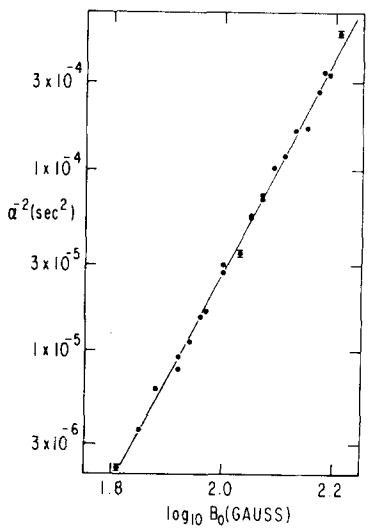

FIG. 14. Dependence of the damping coefficient for the $l=1$ diocotron mode upon B_0. Straight line is a least-squares fit giving $(1/\alpha)^2 \sim B_0^{5.9}$.

because of the possibility of a strong wave-particle interaction. The resonant radius r_s occurs within the tube, $r_s < R$. As previously mentioned, this resonance leads to spatial transport of the resonant electrons. Also, large amplitude diocotron waves can trap resonant electrons, which then execute nonlinear "bounce" orbits due to the radial shear in the drift frequency.

Our experimental investigations have focused upon $l=2$ modes. We launch this mode in the same manner as the $l=1$ mode, that is, with an rf burst at the modal frequency, and find the response in some ways similar to that for $l=1$. The received wave power rises as t_w^2 and the mode can be excited for only a narrow frequency range.

We find excellent agreement between the experimentally determined modal frequency and the real part of the frequency calculated from theory. This agreement is typically within 3%. The theoretical calculation is performed by numerically solving Eq. (5) neglecting the resonant particles. In this calculation we use the measured radial density profile since the frequencies of modes for $l>1$ depend upon this profile. However, the theoretical and experimental damping rates do not agree. The damping rate (γ_c) calculated in the manner described in Sec. IVB is typically of order $|\gamma_c/\omega_r| \sim O(10^{-2})$ whereas, experimentally the damping is observed to be much weaker, $|\gamma/\omega_r| \sim O(10^{-4})$. This discrepancy arises because the waves in this experiment are not linear. The amplitude is sufficiently large so that resonant electrons execute many bounce orbits during the duration of the wave in the plasma. Using the eigenfunction determined in calculating ω_r and the absolute level of the received amplitude we calculate ω_b, finding typical values to be $|\omega_b/\omega_r| \sim O(10^{-1})$.

A logical progression would be first to establish the characteristics of linear waves and then investigate nonlinear effects. We have not performed the linear experiment because we are unable to detect waves of small enough amplitude so that one might expect linear theory to hold. If we require $|\omega_b/\gamma_c| \leq 0.1$, then the peak received amplitude would be roughly 40 dB below the noise level of the phase coherent receiver system used here. The signal level is basically limited by the plasma density.

Nonlinear features of these large amplitude diocotron modes are demonstrated experimentally in Fig. 15. We apply a 20 μsec rf burst to two wall probes and display the log of the received power versus time for different transmitter amplitudes. The curves shown differ by a standard attenuator substitution procedure wherein an attenuator is moved from the receiver line to the transmitter line. In other words, the transmitter is attenuated by some factor and the receiver gain is increased by this same factor. A linear wave will appear unchanged under such a substitution (neglecting receiver noise). These waves are changed, showing nonlinearity. The curves correspond to the attenuation factors listed in the figure. The largest wave, curve (1), corresponds to 0.5 V rms applied to the wall probes.

The damping depends upon the maximum wave ampli-

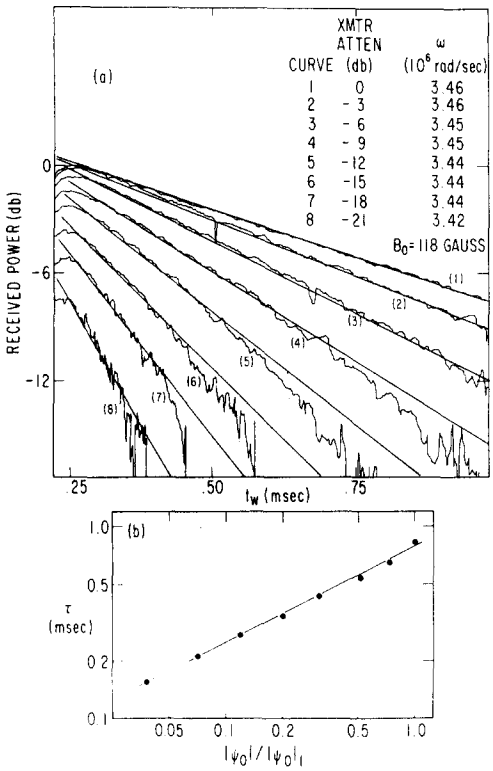

FIG. 15. Transmission and damping of the $l=2$ diocotron mode. (a) Received power for launched modes at different transmitter amplitudes. Receiver gain is increased by the same factor that the transmitter is attenuated. (b) Damping time τ versus the absolute peak received amplitude. The straight line has slope $\frac{1}{2}$, indicating $\tau \sim |\psi_0|^{1/2}$.

tude $|\psi_0|$. Larger waves decay more slowly. Using the lines drawn by eye through the data in Fig. 15(a) we measure the damping time $\tau=\gamma^{-1}$ and plot this time versus $|\psi_0|$ in Fig. 15(b) (logarithmic scales). The line through these points is drawn by eye and has a slope of $\frac{1}{2}$ showing $\tau \propto |\psi_0|^{1/2}$. [Wave amplitude is determined by measuring $|d\psi/dr|_R$, as described in Sec. II and here, we implicitly assume the same $\psi(r)$ profile for each case.]

Using the radial density profile measured for this case, we calculate $\omega_r = 3.37\times10^6$ rad/sec which is within 3% of the (resonant) transmitter frequencies used, being nearest to the frequency of the smallest amplitude wave. We also calculate from the linear theory $|\gamma_c/\omega_r| = 0.02$ in contrast to the experimental results of Fig. 15 where the range shown covers $3.5\times10^{-4} \leq |\gamma/\omega_r| \leq 1.9\times10^{-3}$. For the wave of curve (3) we calculate the bounce frequency at the maximum wave amplitude to be $\omega_b = 3.5\times10^5$ rad/sec. Thus, the bounce time is short compared with the time scale of the wave rise or decay.

The damping rate for the $l=2$ mode is also observed to depend upon the background pressure: higher pressures cause the wave to decay faster. We have investigated this effect for only a limited pressure range near the base pressure. We also note that the damping is insensitive to the length of the trapped plasma in contrast to the $l=1$ mode decay. We have not yet extensively investigated the scaling of the damping with the basic parameters P, B_0, and N because changes in these parameters produce a different plasma density profile; and since the damping is amplitude dependent, a calculation is required to determine the amplitude of the wave within the plasma for each measurement as the parameter is varied.

A possible damping mechanism is transport of the resonant electrons due to collisions with neutrals. The trapped particle orbits execute large radial excursions compared with the size of a Larmor radius. An estimate of this trapping width given by $|\omega_b/(d\omega_e/dr)|_{r_s}$ yields 0.25 cm for the peak level of curve (3) in Fig. 15(a). Collisions which may trap or detrap electrons can cause an exchange of angular momentum between the wave and the resonant electrons. Note that the damping of these waves is only approximately exponential. As the wave amplitude becomes smaller the damping rate increases.

Another nonlinear feature of the data in Fig. 15 is that the transmitter frequency giving the maximum transmission depends upon the transmitter amplitude $|A|$. This is why the frequencies listed differ slightly for each transmitter amplitude. This effect is due to the small shift in the eigenfrequency caused by the wave induced change of the radial density distribution. We find that the received maximum amplitude is not linear in $|A|$, for the smaller amplitude waves $|\psi_0| \propto |A|^{1.5}$. The larger amplitude waves do not show this effect [the maxima for curves (1) and (2) are nearly the same, indicating linearity in $|A|$] because the launched wave amplitude is beginning to saturate as a function of the transmitter amplitude.

Thus for the $l=2$ diocotron mode we find a situation similar to the $l=1$ case in that the idealized linear theory allows accurate calculation of ω_r. We have not yet tested this theory for γ since we are in a nonlinear regime. Nevertheless, damping in this regime has proven very interesting in itself, having an amplitude dependence indicative of trapped particle effects.

V. WAVE-INDUCED TRANSPORT

The launched waves induce transport in the pure electron plasma. The second-order theoretical treatment, or so-called quasi-linear treatment, shows that transport occurs by modifying the unperturbed guiding center distribution function $f^0(r, v_z)$ along the line in the $r - v_z$ plane defined by the resonance condition, $\omega_r - l\omega_e(r) - kv_z = 0$. In changing f^0, resonant electrons move along phase space trajectories defined by $dv_z/dr = -kr\omega_c/l$. (A derivation in planar geometry is given by Stix.[32]) For the usual plasma waves ($l=0$, $k\neq0$), this results in localized velocity transport at all radii for the resonant electrons. For the diocotron waves ($l\neq0$, $k=0$), the result is localized radial transport at all velocities for the resonant electrons. Modes with $l\neq0$, $k\neq0$ produce transport in both phase space directions. The majority of our experimental investigations have dealt with the spatial transport case, that is, transport due to diocotron modes and only this case is presented here. (There must, of course, be some localized axial dependence to the diocotron mode eigenfunction in the experiment since the plasma is axially bounded.)

Radial density profiles taken with and without a launched $l = 2$ diocotron mode are shown in Fig. 16(a). The radial profile showing the effect of the wave was taken after the wave had damped away so the density change shown represents permanent transport and is not due to the coherent density fluctuation of the wave. The wave has moved electrons outward radially which means that the total canonical angular momentum has changed. The torque is applied to the plasma during the launch process.

The wave-induced density change Δn, taken electronically, is shown in Fig. 16(b). These data are taken by a difference technique wherein the wave is launched on every other plasma shot. The resonant radius r_s marked on this figure is determined from $\omega_e(r)$ as calculated from the measured profile. We see that Δn goes through zero at r_s which is what one would expect from a quasi-linear treatment of the resonant particle time-asymptotic transport.

This transport unmistakably results from the collective electric field of the wave in the plasma and is not merely due to the transmitter field. Applying a frequency off that of the mode produces some transport but at a greatly reduced level; Δn when the transmitter is off resonance is typically more than an order of magnitude smaller for the same transmitter amplitude. Much of the transport shown in Fig. 16 occurs while the transmitter is on and also during the initial decay of the mode. However, Δn values taken while the wave is present vary greatly from shot-to-shot. This may merely reflect the fact that the wave phase at the dump time varies from shot-to-shot because the dump cycle and the rf transmitter are free running oscillators. Since the collector is azimuthally localized, it sees the density change resulting from such a phase change.

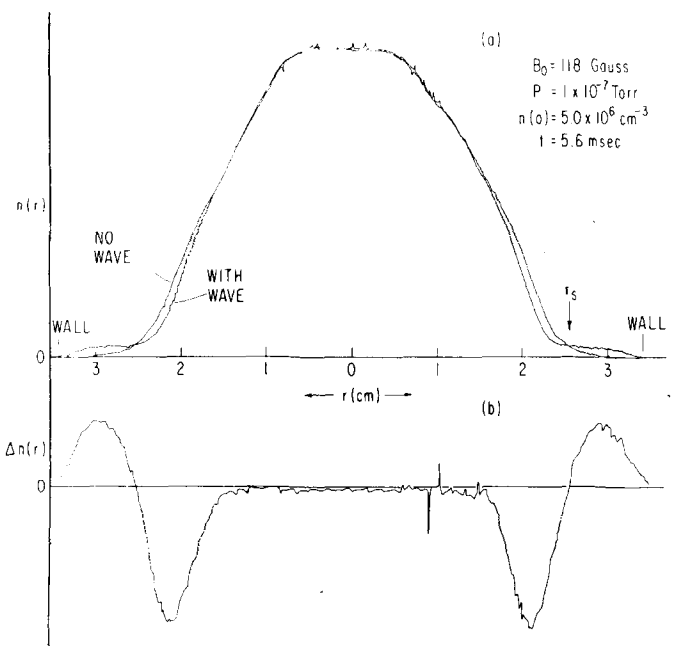

FIG. 16. Launched wave induced transport. (a) Radial density profiles with and without an externally launched $l = 2$ diocotron mode. (b) Wave induced density change taken electronically.

Only after the mode has decayed away is the azimuthally invariant permanent transport observed.

This wave-induced transport is essentially independent of the background neutral density. Doubling the pressure had a negligible effect on the Δn profile of Fig. 16(b). As previously mentioned, the wave damping depends upon neutral pressure. Thus, the rate at which the wave damps does not significantly affect the transport at asymptotic times. The initial perturbation determines this transport while the rate at which this time asymptotic state is reached depends upon neutral pressure. Naturally, transport of the plasma due to neutral collisions subsequently washes out the Δn profile, which, for this case, decayed 50% after approximately 8 msec.

The wave causing the transport shown in Fig. 16 is launched with a transmitter amplitude 5 dB greater than that for curve (1) of Fig. 15(a). We have used such a large wave for this example so that the transport can be clearly seen on the raw radial profiles. With the present Δn technique we can discern transport levels of roughly 0.01 of that shown here. For even this smallest transport level we are still in the large amplitude wave regime in the sense that the bounce frequency is large compared with the damping rate. The transport is observed to scale as the peak received wave power ($\sim|\psi_0|^2$), and so reducing Δn a factor of 100 reduces ω_b only a factor of $(10)^{1/2}$ ($\omega_b \sim |\psi_0|^{1/2}$).

The trapped particle orbits are reflected by the width of the transport region which is comparable to the radial trapping width estimated by $|\omega_b (d\omega_e/dr)^{-1}|_{r_s}$. This width is much larger than the transport width one would predict from a standard quasi-linear (no trapping) theory where the transport width is determined by the autocorrelation time, τ_{ac}, of the mode amplitude envelope. An estimate for the order of magnitude of this width is $|l(d\omega_e/dr)_{r_s} \tau_{ac}|^{-1}$ which is approximately 10^{-2} cm for the case described here. (The collector, collimator diam = 0.30 cm, cannot resolve a width of 10^{-2} cm, but its resolution is adequate to demonstrate that the Δn profiles experimentally obtained are much wider than 0.3 cm.)

Shown in Fig. 17 are Δn profiles (one side only) exhibiting the dependence upon the maximum received power $|\psi_0|^2$. Curve (2) has roughly one-half the peak received power of curve (1) and the same is true of curve (3) relative to curve (2). The amplitude of the peaks in Δn are seen to roughly follow these ratios. Note also that there is a variation in the peak-to-peak radial distance with power. Thus, the width of the asymptotic transport region increases with increasing wave peak power as is expected if the trapping width determines the radial extent of the transport.

The dependence of this transport upon the wave power is shown in Fig. 18, where we have Δn at the radial location of the negative peak of curve (3) in Fig. 17 versus the peak received wave power. Each axis is the output of a lock-in amplifier. The straight lines are drawn by eye to demonstrate the linearity of the scaling. Note that the Δn shapes do change (Fig. 17), but

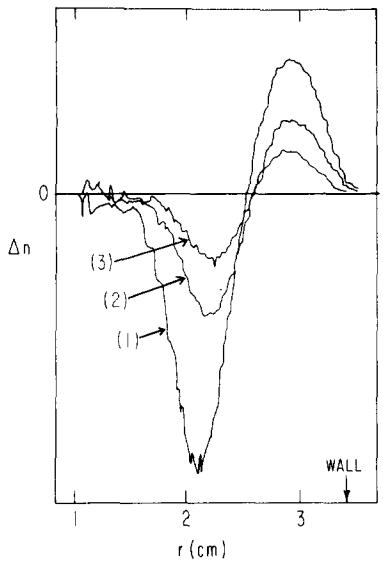

Fig. 17. Wave induced density change with peak received power as the parameter. Curve (3) has approximately $\frac{1}{2}$ the peak power of (1) and (3) has approximately $\frac{1}{2}$ that of (2).

at this radial position the change in density definitely scales as the peak received power.

Thus, the time asymptotic transport exhibits some characteristics predicted by standard quasi-linear theory[30, 32] (but applied to this spatial transport case), even though the resonant electron orbits are highly nonlinear. The magnitude of the transport scales as the square of the wave amplitude and the density perturbation is zero at the resonant radius. However, the width of the transport region is determined by the width of the nonlinear orbits.

As mentioned, we can induce some radial transport even though a mode (i.e., a resonance in transmission)

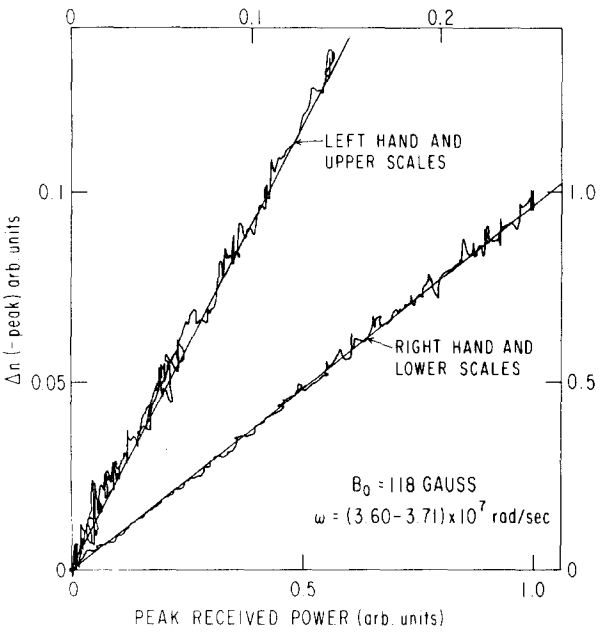

FIG. 18. Continuous measurement of Δn versus the peak received power. The radial position is that of the negative peak of curve (3) in Fig. 17. The straight lines are drawn by eye to show linearity.

is not excited, but much larger transmitter amplitudes are required for transport comparable to that accompanying a mode. For arbitrary ω, we can induce transport at the resonant radius r_s where $\omega = l\omega_e(r_s)$. Interestingly, this transport can be suppressed or enhanced by varying the phase between two launching probes, each at one end of the trapped plasma. We have observed some cases in which electrons are driven inward, up the density gradient, by launching a particular frequency. The inward transport occurs near $r = 0$ under conditions where outward transport also occurs at the edge of the plasma column. This effect has not yet been pursued in detail.

VI. TRANSPORT DUE TO NATURALLY OCCURING DIOCOTRON MODES

The initially trapped plasma is not always as quiescent as described in the previous sections where we presented classical transport and externally induced wave transport. There are regimes determined by the initial conditions of the plasma in which collective effects cause spatial transport. These regimes are determined by source parameters and the details of closing the trap on the plasma. Recalling the discussion of canonical angular momentum one expects that the intraplasma forces arising from these collective fields may only rearrange the plasma distribution subject to momentum conservation. A clear demonstration of such rearrangement is seen in the transport due to a large amplitude $l = 1$ diocotron mode which occurs if the gating pulse closing the electrostatic trap at cylinder A is too fast. For the data presented thus far the plasma was trapped by applying a ramp voltage to close A. If this ramp is shorter than a few times the $l = 1$ wave period, then the wave is "excited." This excitation may be due to electrons which are accelerated into the trapped region (cylinder B) by the gating pulse applied to A. Another possible explanation is that the wave results from the spiral nature of the cathode. Abruptly cutting off this source leaves the plasma at $t = 0$ strongly correlated to this spiral geometry, while slowly cutting it off allows selective filling from the source to smooth out the effect. As yet, we do not know which aspect of the trapping voltage causes the wave excitation.

A case for which the gating pulse is fast and a large $l = 1$ mode is excited is shown in Fig. 19. For the $t = 0$ profile in Fig. 19(a) the density is not maximum at $r = 0$ nor is the profile very symmetric. This is in contrast to the initial profiles previously discussed which resulted from a slow gating of cylinder A. The large diocotron mode is phase locked to the trapping pulse as shown in Fig. 19(b) which displays the density at two different radii as a function of time. The phase locking is evident since the (wavelike) density modulation is periodic in the time interval between the trap and dump pulses (t), starting with the same phase on each shot. (As in all the data, "points" from many shots make up each trace in Fig. 19.) The density fluctuation at $r = r_a$ is the coherent density fluctuation due to this large wave. Phase locking demonstrates that the trapping procedure causes this modal oscillation and it has not grown from noise as an ordinary instability. We find

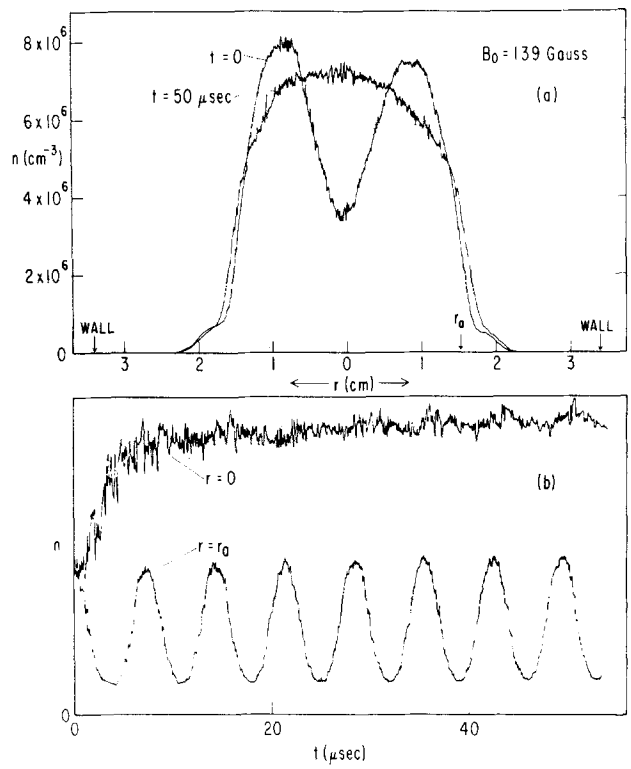

FIG. 19. Spontaneous wave induced transport. (a) Rapid cross field transport due to a large $l=1$ diocotron mode occurring when the gating pulse at cylinder A is too fast. (b) Density versus time at radii indicated. The modulation at r_a is due to the coherent density variation associated with the wave.

that this wave excitation effect is independent of pressure, magnetic field strength, and line density, occurring for all values of these parameters encountered in this experiment.

Spatial transport is also observed here. This is seen in the $t = 50$ μsec profile in Fig. 19(a) where some electrons have filled in the center and some have moved outward. This cannot be collisional transport since this time scale is an order of magnitude smaller than the electron-neutral collision time, which again is much smaller than the electron-electron collision time. Indeed, as seen in Fig. 19(b) the center fills in roughly a wave period. (This is not "resonant" transport since $r_s = R$ for $l = 1$.) We have calculated the canonical angular momentum,

$$P_\theta \simeq \frac{m\omega_c}{2} \int_0^R 2\pi r\, dr\, r^2\, n(r) ,$$

for the two profiles shown and find these values to agree to 5%. We have also calculated the electrostatic potential energy,

$$W \simeq -\frac{e}{2} \int_0^R 2\pi r\, dr\, \phi(r) n(r) ,$$

for the profiles again finding roughly 5% agreement. This is within the confidence level of the calculation which used a density profile which was an average over the asymmetric profiles observed. Thus, this transport takes place conserving canonical angular momentum and electrostatic potential energy. (This calculation neglects the corrections due to the mechanical component of the angular momentum and the kinetic portion of the energy.)

Another example of transport due to collective effects is shown in Fig. 20. In this case the trapping gate at cylinder A is closed slowly, avoiding excitation of the $l=1$ diocotron mode. However, the parameters of the source are different from those used to obtain the comparatively quiescent plasmas discussed in previous sections. Basically, the electron emission density of the source has been increased. The resulting plasma is noisy and the decaying radial density profiles exhibit marked anomalous features.

The profile at $t=0$ in Fig. 20 is smooth although skewed. Within 200 μsec the plasma profile has greatly distorted into the winged shape shown. This anomalous shape persists while the bulk of the plasma decays due to transport occurring as a result of collisions with background neutrals. Here, the neutral pressure is at the base level. We have observed such anomalous features over three orders of magnitude in background pressure. Of course, at higher pressures the bulk transport rate (loss of electrons to the walls) is faster. Keep in mind that these profiles are taken over many plasma shots, showing that the anomalous shape develops the same on each shot.

This anomalous shape is due to an $l=2$ diocotron mode, but now this mode has not been excited by a transmitter. The modal frequency is measured with a narrow band receiver system. These data are shown in Fig. 21 where we plot the received amplitude at the indicated frequency (bandwidth = 10 kHz) versus time. The strong peaks occur when the modal frequency sweeps through the receiver pass band. The arrows on the profiles in Fig. 20 mark the location of the resonant radius at that time, that is, where $\omega_{sp} = 2\omega_e(r_s)$, where $\omega_{sp} = 2\pi\times$ (frequency of spectral peak). The effect of the wave is again to transport particles radially.

Calculation of ω_r from linear theory gives good agreement with the measured value. For the $t=200$ μsec profile there is a root at $\omega_r = 1.10\times 10^7$ rad/sec while the measured spectral peak is at $\omega_{sp} = (1.04\pm 0.02) \times 10^7$ rad/sec. In order to avoid the pole, this calculation was performed on a slightly modified version of the measured profile. Specifically, we use a profile which is flat ($dn/dr = 0$) over the region where the true profile dips.

As yet, we do not know the cause of this mode excitation, or the cause of its persistence as the plasma decays away. One difference between these profiles and the quiet ones is that here the central density is initially larger. As we reduce the source emission we find a continuous transition from this case to the quiet cases. We also find that the length of the trapped plasma matters. Changing the length changes the details of the anomalous density profiles.

VII. SUMMARY

The wave and transport properties of the pure electron plasma have been experimentally studied. This plasma

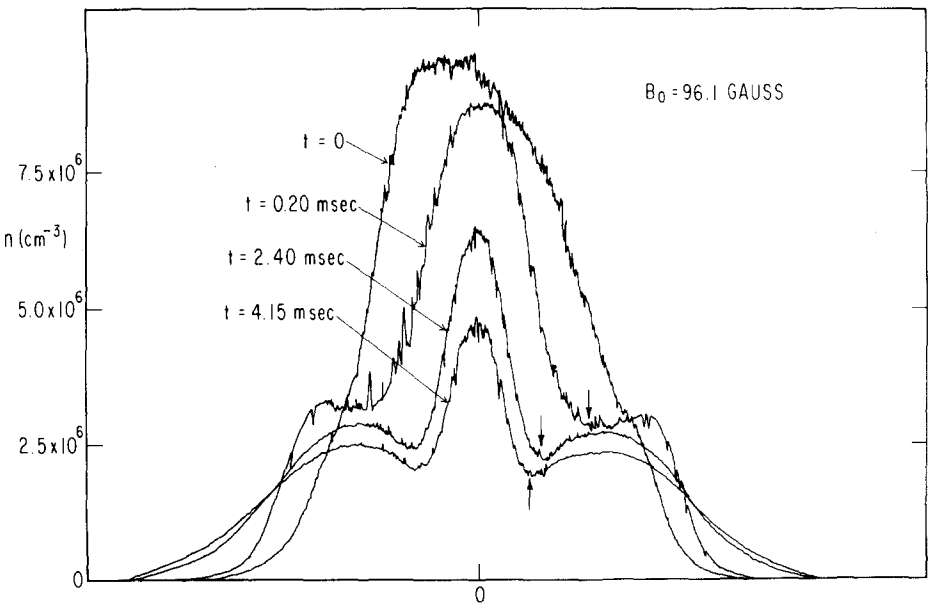

FIG. 20. Radial density profiles showing anomalous transport due to a naturally occurring $l = 2$ diocotron mode. Arrows mark r_i for which $\omega_{sp} = 2\omega_e(r_i)$.

is easy to make and can be captured in fields of relatively simple geometry: radial confinement is provided by a static magnetic field while axial confinement is by electrostatic fields. Very long confinement times are possible because an external torque must be applied to this captured plasma in order to transport a non-negligible fraction of the electrons across the magnetic field to the wall of the surrounding cylinder. An external torque can be applied through collisions with background neutrals and through imperfections in the geometry of the confinement system. These effects can be made very small and mechanisms causing transport can be externally induced and isolated.

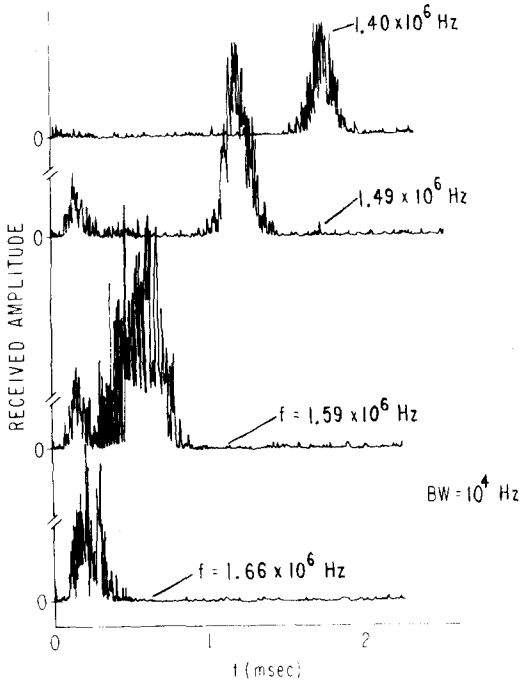

FIG. 21. Received amplitude versus time at the indicated center frequency.

We have investigated classical transport due to electron-neutral collisions by adding neutral gas to the system thereby raising the neutral density far above the base level. We have verified the basic scaling of the decay time, $\tau \sim B^2/P$, and also verified mobility effects due to the space charge electric field in this singly charged plasma. Comparison of the time evolution of the radial density profile with the prediction of the kinetic theory of Douglas and O'Neil[14] gives good agreement.

We have also induced transport by externally launching diocotron waves. We observe the striking signature of spatial localization of the transport due to these waves. The time asymptotic transport scales as the peak power of the wave over two orders of magnitude. Also described are cases in which naturally occurring diocotron modes cause strong spatial transport.

Launched diocotron modes were investigated experimentally. We find the measured modal frequency agrees well with that calculated from linear theory. For the $l = 2$ mode, the wave amplitude is large in the sense that resonant electrons execute trapped particle orbits in space and the damping is nonlinear. The damping has a clear dependence on the peak wave amplitude: $\gamma \sim |\psi_0|^{-1/2}$. In the case of the $l = 1$ mode for which no electrons are exactly resonant, we find that the wave amplitude decays as $\psi(t) \sim \psi_0 \exp(-\alpha^2 t^2)$. As yet, we have no detailed theoretical description for these signatures in the damping rates.

ACKNOWLEDGMENTS

Throughout the course of this research we have enjoyed numerous and enlightening discussions with Professor T. M. O'Neil, Professor W. B. Thompson, and Dr. M. H. Douglas. We thank Dr. Douglas and Professor O'Neil for the use of their computer program for numerical solution of their reduced transport equation. Expert technical assistance was provided by G. A. Smith and also by L. D. May in the early phases

of this work.

This work was supported by National Science Foundation Grant Nos. PHY73-05125-A03 and PHY77-02631.

[1]A. W. Trivelpiece, Comm. Plasma Phys. Control Fusion **1**, 57 (1972).
[2]R. C. Davidson, *Theory of Nonneutral Plasmas* (Benjamin, Reading, Mass., 1974).
[3]J. S. deGrassie and J. H. Malmberg, Phys. Rev. Lett. **39**, 1077 (1977).
[4]J. H. Malmberg and J. S. deGrassie, Phys. Rev. Lett. **35**, 577 (1975).
[5]R. C. Davidson and N. A. Krall, Phys. Fluids **13**, 1543 (1970).
[6]G. C. MacFarlane and H. G. Hay, Proc. R. Soc. London Ser. B **63**, 409 (1953).
[7]O. Buneman, in *Crossed Field Microwave Devices*, edited by E. Okress (Academic, New York, 1961), Chap. 5.
[8]J. R. Pierce, IRE Trans. Electron. Devices **ED-3**, 183 (1956).
[9]O. Buneman, J. Electron. Coltrol **3**, 507 (1957).
[10]R. W. Gould, J. Appl. Phys. **28**, 599 (1957).
[11]W. Knauer, J. Appl. Phys. **37**, 602 (1966).
[12]R. H. Levy, Phys. Fluids **8**, 1288 (1965).
[13]R. J. Briggs, J. D. Daugherty, and R. H. Levy, Phys. Fluids **13**, 421 (1970).
[14]M. H. Douglas and T. M. O'Neil, Phys. Fluids **21**, 920 (1978).
[15]R. C. Davidson, J. Plasma Phys. **6**, 229 (1971).
[16]T. M. O'Neil and C. F. Driscoll, Phys. Fluids **22**, 266 (1979).
[17]R. H. Levy, Phys. Fluids **11**, 920 (1968).
[18]C. A. Kapetanakos and A. W. Trivelpiece, J. Appl. Phys. **42**, 4841 (1971).
[19]T. Hsu and J. L. Hirshfield, Rev. Sci. Instrum. **47**, 236 (1976).
[20]J. S. deGrassie, Ph.D. dissertation, University of California, San Diego (1977).
[21]G. J. Schulz, J. Appl. Phys. **28**, 1149 (1957).
[22]W. P. Allis, in *Handbuch der Physik* (Springer-Verlag, Berlin, 1956), Vol. XXI, p. 383.
[23]A. Gilardini, *Low Energy Electron Collisions in Gases* (Wiley, New York, 1972).
[24]H. F. Webster, J. Appl. Phys. **26**, 1386 (1955).
[25]C. C. Cutler, J. Appl. Phys. **27**, 1028 (1956).
[26]C. A. Kapetanakos, D. A. Hammer, C. D. Striffler, and R. C. Davidson, Phys. Rev. Lett. **30**, 1303 (1973).
[27]J. D. Daugherty, J. E. Eninger, and G. S. Janes, Phys. Fluids **12**, 2677 (1969).
[28]W. Clark, P. Korn, A. Mondelli, and N. Rostoker, Phys. Rev. Lett. **37**, 592 (1976).
[29]L. Landau, J. Phys. (USSR) **10**, 25 (1946).
[30]J. H. Malmberg, T. H. Jensen, and T. M. O'Neil, in *Plasma Physics and Controlled Nuclear Fusion Research* (International Atomic Energy Agency, Vienna, 1969), Vol. I, p. 683.
[31]T. M. O'Neil, Phys. Fluids **12**, 2255 (1965).
[32]T. H. Stix, Phys. Fluids **10**, 1601 (1967).
[33]B. F. Fried and S. Conte, *The Plasma Dispersion Function* (Academic, New York, 1961).
[34]S. A. Prasad and T. M. O'Neil, Phys. Fluids **22**, 278 (1979).